A Modal Contribution Metric for Quantifying Small-Signal Variability in Power Systems with Converter-Interfaced Generation

A Modal Contribution Metric for Quantifying Small-Signal Variability in Power Systems with Converter-Interfaced Generation

Luke Benedetti, *Member, IEEE*, Panagiotis N. Papadopoulos, *Member, IEEE*, and Agustí Egea-Àlvarez, *Member, IEEE*

***Abstract*—Power system dynamic behaviour is changing drastically with the disconnection of synchronous generation and increasing connection of converter-interfaced units, which is not necessarily captured by traditional static grid strength metrics. This paper uses the modal superposition concept to derive metrics and information with respect to locational variability, defined in terms of the maximum deviation of system variables in different network locations. Going beyond typical grid strength metrics, the analysis considers voltage magnitude and frequency variability separately, reflecting the complexities arising from the transition to power electronic control dominated power system dynamics. A further benefit of the approach is the derivation of a clear relationship between the variability of output variables and specific modal interactions via their contribution to the response. The Kundur two-area, four-generator system is utilised and investigations are performed with the integration of grid-following and grid-forming converters to compare with the standard synchronous generator case. The methodology and suggested metric reflects the independent voltage and frequency variability trends across different locations of disturbance and observation across the network. Also exhibited is the use of the proposed method to focus on the characteristics and causes of variability at different timescales.**

***Index Terms*—Converter, dynamics, eigenvalue, eigenvector, frequency, location, small-signal, strength, system, voltage.**

I. Introduction

With the integration of converter-interfaced generation (CIG) and the subsequent surge of complexity in power system dynamics, new approaches and appropriate metrics for power system analysis are required. The limitations of short-circuit ratio (SCR) based grid strength indicators are being discussed [1]–[3], necessitating new approaches for the determination of locational information with respect to the magnitude of changes expected in power systems variables.

The increasing complexity of the analysis of power systems associated with including CIG is highlighted in [4], [5]. In addition, complex control strategies are not reflected in proxy steady state indices such as SCR [1]. The implementation and analysis of small-signal models (SSMs) [6], as well as the inclusion of relevant dynamic information, suggests the possibility to extract useful locational trends and offer insights into complex dynamic behaviours. This is related to the *small-signal system strength* concept as discussed in [7].

A further motivating factor is the decoupling of voltage magnitude and frequency variability, something that is not necessarily described by traditional system strength based metrics. In traditional synchronous generator (SG) dominated systems, frequency and voltage regulation were closely linked to the generation capacity and inertia since both services were typically offered by SGs. This cohesion cannot be assumed with CIG and the wide range of control possibilities. The separation of the voltage magnitude and frequency forming aspects are discussed in more detail in [5], [8], [9]. In this context, the locational variability of both voltage magnitude and frequency are investigated separately in this paper. A further consequence of the integration of CIG is the concept of increasing variability in regional frequency [10]. To address this, the local frequency is estimated at each bus using the frequency divider formula (FDF) introduced in [10].

Improvements to system strength metrics have been attempted, with those including small-signal considerations focusing on impedance modelling and singular metrics based on stability margins or impedance coupling [2], [3], [7], [11]. In particular, the impedance margin ratio, generalised short-circuit ratio, and grid strength impedance metric (GSIM) are examples of the state-of-the-art in this regard. The impedance margin ratio [7] and generalised short-circuit ratio [11] are based on stability margins with the former considering the allowed variation of the impedance and the latter using eigenvalue-based stability. The grid strength impedance metric offers an alternative to SCR whereby the perspective of electrical distance from an ideal voltage source is maintained but the impedance of CIG and its control are incorporated into the calculation of the metric [2], offering better reflection of their impact on voltage strength. In addition, their work expands the consideration of system strength across the frequency spectrum, going beyond simply the fundamental frequency. These metrics are proving more adequate in reflecting CIG impact on stability/oscillation damping [12]. However, they do not consider the decoupling of voltage magnitude and frequency, nor do they provide

L. Benedetti (during the undertaking of this work) and A. Egea-Àlvarez are with the Department of Electronic and Electrical Engineering, University of Strathclyde, Glasgow, Scotland (email: agusti.egea@strath.ac.uk).

P. N. Papadopoulos is with the Department of Electrical and Electronic Engineering, University of Manchester, Manchester, UK (email: panagiotis.papadopoulos@manchester.ac.uk). L. Benedetti is also now affiliated with this institution (email: luke.benedetti@manchester.ac.uk).

Financial support is acknowledged from an EPSRC Student Excellence Award Studentship 2437798 (L. Benedetti) and a UKRI Future Leaders Fellowship MR/S034420/1 (P. N. Papadopoulos). All results can be fully reproduced using the methods and data described in this paper and provided references.

specific information regarding the variability of any given output signal (which in this work is found to not necessarily relate to traditional stability metrics) and the contributing dynamic interactions.

Notably, some of the recently introduced grid strength metrics are developed in such a manner that they relate to system stability margins. There is of course a relation between grid strength and stability, whereby a stronger grid *implies* a higher stability margin. However, in this work we propose a quantification approach based on variability (i.e., how much a variable deviates) which can be directly linked to the concept of strength. Note, in traditional grid strength metrics such as SCR–and some more modern approaches such as GSIM–the grid strength is considered from an (in)variability perspective whereby the electrical distance from an ideal voltage source represents strictness of control of the voltage phasor (magnitude and frequency) and therefore less variability of said phasor. That is, these metrics were aiming at offering a quantification of how much or not the voltage and frequency will vary. Our approach provides a more direct measure of how the voltage and/or frequency (or any output variable of interest) will vary in the domain-response for any given disturbance. Furthermore, existing electrical distance-based grid strength metrics suggest either variability or invariability regardless of disturbance type or location, as well as the lack the decoupling between "strength" of voltage and frequency (as previously discussed). We have seen in this work that this can in fact have a significant impact on the variability from one location (or output variable) to another.

The method proposed in this paper comes from a modal decoupling perspective with relation to the concepts of small-signal observability and controllability. Similarly, within the framework of dynamic grid flexibility [13], the inertial distribution index is proposed. This index uses the mode shape observability of the "most global" mode to extract information regarding the inertial distribution of the system. However, although undoubtedly useful, this index is focused on a single mode (and output). Consequently, it has the potential to miss variability information related to other modes. This is especially true considering the changing dynamic timescales and control approaches associated with CIG. [14] has relation to the inertial distribution concept whereby it can consider the locational relation between a single mode and specified outputs but through their derived participation factors of algebraic variables. Additionally, the output of interest is not focused on the locational frequency but is applied to any algebraic variable or output.

Compared to prior works described above, the metric and method proposed in this paper focuses on capturing locational information that drive the variability of system output variables (i.e., frequency and voltage). This can be extracted using the modal superposition concept, without neglecting the effect of multiple modes that can affect specific power system variables. This involves defining a metric based on the analytical solution of the individual modal responses and their contribution to the system output variable of interest, the details of which are dependent on the corresponding eigenvalues and eigenvectors as well as the excitation–i.e., utilising concepts from observability and controllability analysis [15], [16] but extending these concepts to enable tracing the dynamic interactions that affect the variation of output variables which in turn allows for the definition of a variability metric. That is, going beyond an approach similar to participation factors for output variables by quantifying and understanding directly the impact of a disturbance to the output magnitude.

Consequently, the main aim of the proposed method is to determine a metric to analytically quantify the impact of disturbances across different locations of the system on the time-domain response of relevant power system output variables (i.e., voltage and frequency), referred to as the outputs' *variability*. This provides a quantification of small-signal grid-strength linked to the physical meaning of the amplitude of deviations observed in time domain simulations, while accounting for the detailed dynamic responses of systems, including the response of CIG. The resulting distinct contributions of this paper are:

- An alternative viewpoint for system strength from the perspective of small-signal variability. A method is proposed for the analysis of locational small-signal voltage and frequency variability considering different disturbance types and locations. This includes a metric to quantify small-signal variability based on modal superposition. It allows to take into account detailed aspects related to system dynamics and interactions, contrary to conventional system strength metrics.
- The method offers a clear indication of the contribution of a specific mode/interaction to the variability of the time domain response of any given output through the analytical calculation of the maximum deviation of the decoupled modal response.
- The method also offers the capability to extract distinct variability trends across different timescales and the respective fast or slow dynamic modes that contribute.
- An analysis of the impact of the introduction of CIG with both grid-following (GFL) [17], [18] and grid-forming (GFM) [9] control on the locational small-signal variability of the system is carried out.

The remainder of the paper is structured as follows: Section II details the relation between modal responses and power system output variables as well as deriving the analytical solution of the response and the corresponding variability metric; Section III describes the dynamic modelling of the power system and relevant components; Section IV outlines the specific test cases; Section V displays the corresponding results; and Section VI concludes the paper.

II. Methodology: Introducing a Power System Variability Measure

A. Defining Variability

In this work, we define variability based on the maximum deviation of power system output variables in their time domain responses. Since small-signal (impulse) disturbances are considered, the maximum deviation is taken from the initial operating value of the output variable of interest. The motivation behind this is to derive metrics and perform

relevant analysis that identifies situations where power system variables (e.g., voltage and frequency) throughout different parts of a system tend to exhibit high deviations from their initial values. Such situations could indicate possible limit violations, system stress and generally the tendency of high amplitude oscillations. This definition of variability therefore relates to a way of quantifying system strength while taking into account detailed dynamic responses, becoming especially relevant in power systems with high converter penetration.

Also, to reiterate one of the key points from the introduction, the variability is related to the idea of strength whereby an increase in the latter means a decrease of the former. However, strength is also sometimes linked to the idea of stability and therefore stability margin metrics are used in some more modern grid strength quantifications. Therefore, it should be highlighted that although there is a relationship between variability and stability through the idea of strength, they are not directly linked and a decrease in variability does not necessarily mean an increase in stability (margin). For example, a damped oscillation with a high amplitude would have high variability but not necessarily low stability margin. Such a disconnect between variability and stability margin is further highlighted in Section V-E.

B. Decoupled Modal Responses on System Output Variables

After linearisation around an operating point, a power system can be represented by a dynamic model in state-space format as in (1),

$$\begin{aligned} \dot{\Delta \boldsymbol{x}} &= \boldsymbol{A}\Delta\boldsymbol{x} + \boldsymbol{B}\Delta\boldsymbol{u} \\ \Delta\boldsymbol{y} &= \boldsymbol{C}\Delta\boldsymbol{x} + \boldsymbol{D}\Delta\boldsymbol{u}, \end{aligned} \tag{1}$$

where $\boldsymbol{x}$ is the vector of (N) states, $\boldsymbol{u}$ is the vector of (N_i) inputs, and $\boldsymbol{y}$ is the vector of (N_o) outputs. The prefix Δ denotes a small deviation and the dot operator represents differentiation with respect to time. The matrices $\boldsymbol{A}$, $\boldsymbol{B}$, $\boldsymbol{C}$ and $\boldsymbol{D}$ correspond to the state matrix, input matrix, output matrix and feed-forward matrix, respectively [15], [19].

From the small-signal model (SSM), eigenvalues and eigenvectors can be determined, with relation as in [15],

$$\boldsymbol{A}\boldsymbol{\phi} = \boldsymbol{\phi}\boldsymbol{\Lambda} \tag{2}$$

$$\boldsymbol{\psi}^{\intercal}\boldsymbol{A} = \boldsymbol{\Lambda}\boldsymbol{\psi}^{\intercal}, \tag{3}$$

where $\boldsymbol{\phi}$ and $\boldsymbol{\psi}$ are the matrices containing the right and left eigenvectors in their columns, respectively, and $\boldsymbol{\Lambda}$ gives the diagonal matrix of eigenvalues, $\{\lambda_1, \lambda_2, \ldots, \lambda_N\}$.

The free response of a linear dynamic system [15] is represented by a superposition of individual modal responses:

$$\begin{aligned} \Delta x_i(t) = \phi_{i,1}c_1 e^{\lambda_1 t} + \phi_{i,2}c_2 e^{\lambda_2 t} + \cdots \\ + \phi_{i,n}c_n e^{\lambda_n t} + \cdots + \phi_{i,N}c_N e^{\lambda_N t}, \end{aligned} \tag{4}$$

$$c_n = \boldsymbol{\psi_n}\Delta\boldsymbol{x}\,(\boldsymbol{0}), \tag{5}$$

$$\Delta y_j = \left[\frac{\delta y_j}{\delta x_1}, \cdots, \frac{\delta y_j}{\delta x_n}, \cdots \frac{\delta y_j}{\delta x_N}\right]\Delta\boldsymbol{x} = \boldsymbol{C_j}\Delta\boldsymbol{x}, \tag{6}$$

where $\Delta x_i(t)$ is the time-domain response of the i^{th} state whose relation to the output is specified in (6). In this work, the output Δy_j is either the voltage magnitude or frequency at any bus of interest, with the latter calculated using the FDF [10] (see Section III for more information). The initial deviations $\Delta\boldsymbol{x}\,(\boldsymbol{0})$ will depend on the chosen disturbance type (active power load disturbance in this work) and location. The combined mode shape, $\phi_{i,n}$, and excitation terms–i.e., c_n, which relates the disturbance to the excitation of the mode in (5) through the controllability, quantified by the left eigenvector–constitute the amplitude and phase of the individual mode responses (before damping), as seen in (4). If we focus on a single state, i, then the unitary excitation of only this state, $\Delta x_i(0)$, will cause the coefficient terms of each modal response to be the corresponding participation factor [20].

Knowing the relationship between states and outputs as in (6), we can then determine the output as a superposition of modal responses with

$$\begin{aligned} \Delta y_j(t) &= \sum_{i=1}^{N} C_{j,i}\Delta x_i(t) = \sum_{i=1}^{N}\sum_{n=1}^{N} C_{j,i}\phi_{i,n}c_n e^{\lambda_n t} \\ &= \sum_{n=1}^{N}\left[\sum_{i=1}^{N} C_{j,i}\phi_{i,n}\right] c_n e^{\lambda_n t} = \sum_{n=1}^{N} \Phi_{j,n}c_n e^{\lambda_n t}, \end{aligned} \tag{7}$$

where $\boldsymbol{\Phi}$ can be considered the *output mode shape* which is compared to the right eigenvectors from (2) but for any given mode's observability on the chosen outputs instead of the system states. Note that, if we focus on a single output, j, and consider the unitary excitation of each state, i, prior to performing the sum in the square brackets of (7), the resultant modal coefficient term for each mode is found to be the *participation factors of algebraic variables* derived in [14]. This can be expressed for each mode, n, as

$$\pi_{j,n} = \sum_{i=1}^{N} C_{j,i}\phi_{i,n}\psi_{i,n}. \tag{8}$$

C. Calculating the Maximum Deviation (or Contribution) of Decoupled Modal Responses on Output Variables

Having decoupled the modal responses with respect to system output variable (voltage or frequency), the maximum deviation of each modal response can be determined as a measure of their contribution to the output small-signal variability. Hence, we calculate the maximum deviation of each modal response whose characteristics are described fully by their eigenvalue and eigenvectors as well as the excitation.

As can be seen from (4), the time-domain response for each mode can be described either by an exponential reduction, in which case the time at which the maximum deviation occurs will be zero seconds (the occurance of the disturbance), or an oscillation whose amplitude is exponentially decaying. Whether it is the former or latter depends on whether the eigenvalue is real or complex, respectively. The oscillatory response can be described in familiar mathematical terminology as

$$\chi(t) = Ae^{\sigma t}cos(\omega t + \theta), \tag{9}$$

with A, θ, σ, and ω being the amplitude, initial phase, damping constant, and oscillation frequency, respectively.

In order to get from a mode contribution in (4) to the form in (9) we can consider that an oscillation comprises of two eigenvalues, one with positive and one with negative frequency. Similarly, the polarity of the complex values in the corresponding eigenvectors will be reversed with the result being that the initial phase will also be opposite [15]. Consequently, for output j and mode n,

$$A = 2|\Phi_{j,n}c_n|, \tag{10}$$

$$\theta = \angle\Phi_{j,n}c_n, \tag{11}$$

$$\lambda_n = \sigma \pm j\omega. \tag{12}$$

Unlike an exponential decay, the maximum deviation of (9) will not necessarily occur at zero seconds. However, the simple second order response allows us to solve analytically the time at which the maximum deviation/value will occur. Note, this solution is dependent on the assumption that we have constant, real values for A, σ, and θ, with the additional requirement that σ is positive. We want to determine the first instance at which the derivative of (9) is zero, i.e., the first maxima or minima of the solution, because the absolute value of any succeeding maxima or minima will be smaller due to the damping of the mode. The resultant equation is,

$$\frac{d\chi(t)}{dt} = Ae^{\sigma t}(\sigma cos(\omega t + \theta) - \omega sin(\omega t + \theta)) = 0, \tag{13}$$

which can be simplified to

$$cos(\omega t + \theta) - \frac{\omega}{\sigma} sin(\omega t + \theta) = 0. \tag{14}$$

Solving (14) for t gives

$$t = \frac{n\pi - \left(\theta + jlog\left(\pm\frac{\sqrt{-\sigma^2-\omega^2}}{\sigma+j\omega}\right)\right)}{\omega}. \tag{15}$$

The choice of value for n is dependent on the fact that we are considering a causal system (i.e., $t \geq 0$) and hence,

$$n\pi - \theta - jlog\left(\pm\frac{\sqrt{-\sigma^2-\omega^2}}{\sigma+j\omega}\right) \geq 0, \tag{16}$$

and considering the positive damping of the oscillation, we require the first integer value of n for which this criterion is met, resulting in

$$n = \left\lceil \left(\theta + jlog\left(\pm\frac{\sqrt{-\sigma^2-\omega^2}}{\sigma+j\omega}\right)\right)/\pi \right\rceil, \tag{17}$$

where the ceiling operator is $\lceil\square\rceil$. Note, considering the dual solution to (15), there will be two solutions to (17) but as long as the value of n is matched to the corresponding equation then the result of (15) will be the same. That is, the $\pm$ operator can be replaced with either a $+$ or a $-$, provided consistency is ensured throughout. Therefore, we can determine that the maximum deviation of the solution to (9) will occur at either the positive solution of (15), i.e., the first maxima/minima, or at the instance of the disturbance.

The next step is to relate the known parameters, i.e., the eigenvalues and eigenvectors, in (7) to the parameters required to solve (15) and substitute the resultant equation back into (9). This is achieved with reference to (10) to (12) and by substituting everything back into (9) we get the final maximum deviation value associated with any given mode, which is

$$\Delta y_{j,n}^{max} = 2\left|\Phi_{i,n}c_n\right| e^{\sigma t_{max}} cos\left(\omega t_{max} + \angle\Phi_{i,n}c_n\right), \tag{18}$$

where t_{max} is either calculated with (10) to (12), (15), and (17), or $t_{max} = 0$ s, depending on which choice of t_{max} gives the larger value of $\left|\Delta y_{j,n}^{max}\right|$. Note, for a real-valued mode, the maximum deviation occurs at 0 s and is equivalent to $A/2$ with respect to (10).

D. Deriving a Variability Metric

The maximum deviations of the decoupled modal responses, used to reflect the modal contributions to a single output, can be condensed to a single metric to enable comparison between several outputs. Particularly, this gives a proxy for the variability (maximum deviation) of voltage magnitude or frequency at each bus location. The adopted approach takes the maximum absolute value of maximum deviation, or the Maximum Absolute Modal Contribution (MAMC), as the indicator. This is described for the j^{th} output as

$$\text{MAMC}_j = max\left(\left|\Delta \boldsymbol{y_j^{max}}\right|\right), \tag{19}$$

where $\Delta \boldsymbol{y_j^{max}}$ is the vector for output j whose entries are the modal response maximum deviations calculated as described in Subsection II-C.

Prior to the extraction of the MAMC through (19), there is the possibility to focus on modes with specific characteristics. E.g., if specific damping timescales are of interest, a weighting of zero can be applied to any mode whose damping time constant is outwith that of interest. This provides an indication of the variability differences depending on timescales as well as an understanding of the different modes that dominate at these different timescales (as later presented in Subsection V-F). It should be noted that the main assumption of (19) is that the output response will closely resemble the response of the mode which provided the MAMC: neglecting potential constructive or destructive interference caused by the remaining modes.

E. Application of Disturbance

For the input disturbances in this paper, a negative injection of current corresponding to 0.1 pu active power is applied at each bus. The relation between the disturbance of interest and the excitation terms are through the initial state deviations, $\Delta\boldsymbol{x}\,(\mathbf{0})$. As a proxy for the initial state deviations, the input matrix is used in (20) to determine the rate of change of any given state resulting from the input disturbance which in turn is assigned to the initial deviations as $\Delta x_n(0) := \Delta\dot{x}_n$.

$$\Delta\dot{x}_n = \left[\frac{\delta\dot{x}_n}{\delta u_1}, \cdots, \frac{\delta\dot{x}_n}{\delta u_{N_i}}\right]\Delta\boldsymbol{u} = \boldsymbol{B_n}\Delta\boldsymbol{u} \tag{20}$$

If an impulse disturbance is considered, the forced response collapses to the same representation as the free response with such proxy initial states (see Chapter 4.1 of [21]).

It may be considered more appropriate to use the forced response based on a step disturbance to extract a variability indicator as this represents better an actual disturbance that might occur on the system. However, in doing this, the eigendecomposition of the output becomes significantly more complex, concealing the useful link between variability and system interactions (as the impact of natural system changes also influences the time-domain response). Extension of this method to step disturbances is reserved for future work. Furthermore, the choice of disturbance variable will also influence the outputs' variability. While we choose a specific variable to introduce disturbances (current injection) when presenting our results in this paper, the proposed method can accommodate different disturbances such as voltage magnitude perturbations. Future work could systematically investigate the impact of such different disturbances.

III. Modelling

All modelling was completed in MATLAB 2021b [22]. The SGs are balanced 8^{th} order models [19], equipped with the DC1A exciter and AVR as in Example 12.6 of [15].

Common to GFLs and GFMs are power measurement filters and output RLC filter [17]. The converter is averaged with switching transients and PWM delay neglected [18]. Each machine is implemented in a dq0 reference frame (converter control is d- to a-axis aligned with q axis lagging 90^o) and the electrical system is in the frame of the chosen reference machine. The voltage and current signals require a geometric transformation between frames at the connection points [18].

For the figures in the following subsections, $\boldsymbol{i_{cv}}$ and $\boldsymbol{i_g}$ are the currents before and after the filter capacitor (flowing out of the converter), respectively. $\boldsymbol{v_{cv}}$ and $\boldsymbol{v_m}$ respectively refer to the voltages at the output of the converter switches and the filter capacitor. Finally, P_e and Q_e are the active and reactive power at the point of common coupling (PCC), after filtering.

Additionally, the passive network, stator, and converter output filter elements have been modelled with the quasi-static assumption [19], [15]. Before making this simplification, the impact on the eigenvalues of the systems were checked and it was confirmed that the dynamics included in the quasi-static model (i.e., all except electromagnetic network transients) matched closely their counterparts in the EMT [5] model. Consequently, the focus of our study is mostly on converter and generator dynamics and how these can affect the variability of outputs. Although, theoretically network dynamics could be included as part of the proposed methodology, this might lead to challenges related to modal combination at very fast timescales. Some discussion on related aspects is provided in Section V-A2 but mostly falls out of the scope of this paper and is reserved for future work. Furthermore, provided the focus of an investigation is on converter and generator dynamics (as is the case in this paper), the ability to separate the timescales on which the variability is analysed, as in Section V-F, would also be expected to alleviate potential issues.

As discussed previously, the frequency divider formula [10] was adopted to obtain an estimation of the frequency at each bus. In particular, this includes consideration of the SG internal impedance and the GFM coupling filter. For the frequency at a bus with GFL converter, the phase-locked loop (PLL) measurement is used as input to the formula (note, this is an estimation and this should be taken into consideration when analysing results).

A. Grid-Following Converters

The GFL used in this work, displayed in Fig. 1, is a standard vector current control consisting of PI-based active power controller (APC) and reactive power controller (RPC), inner current controller (ICC), and a phase-locked loop (PLL). The tuning of the ICC is based on the modulus optimum technique [23], whereas the APC, RPC, and PLL are tuned to maintain stability in a weak grid with the approach in [17].

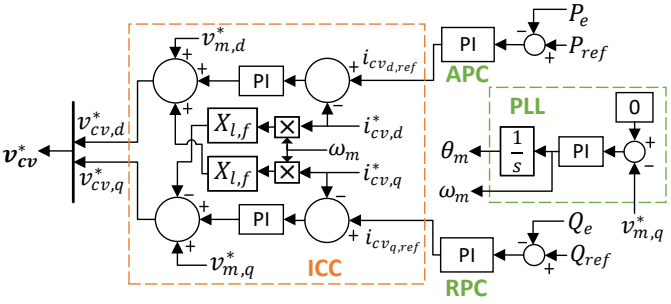

Fig. 1: Grid-following control system block diagram.

B. Grid-Forming Converters

The GFM used in this work, displayed in Fig. 2, consists of an outer loop which synthesises the voltage phasor through an active power controller (APC), in the form of a virtual synchronous machine (VSM) [9], a voltage magnitude controller (VMC), in the form of a reactive power-voltage droop [24], and a virtual inductance [24]. The choice of virtual inertia constant, H, of 6.5 s ensures proper comparison with the SGs. Note, the active power measurement is not filtered since the VSM swing equation effectively achieves this [9].

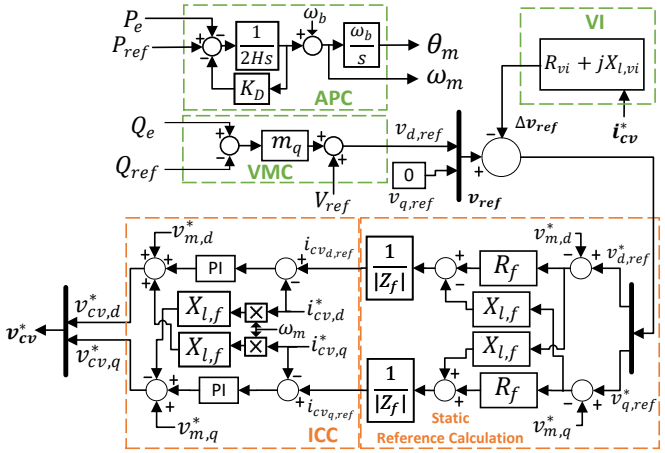

Fig. 2: Grid-forming control system block diagram.

The GFM also adopts a cascaded ICC which requires a static reference calculation based on the coupling filter impedance $Z_f = R_f + jX_{l,f}$ [25].

IV. Test Cases

Due to its clearly distinct areas, the Kundur two-area test system [15] was chosen to be studied. This incorporates two similar areas with a weak tie line between them as displayed in Fig. 3. All synchronous generator and system information

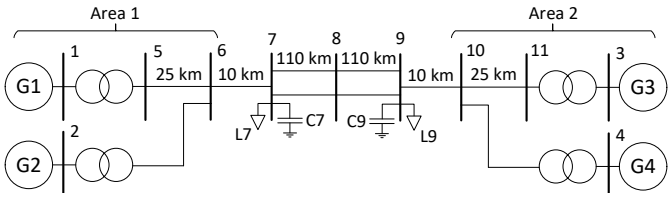

Fig. 3: Kundur's two-area four-generator system. Figure adapted from [15].

is available in [15]. This SG-only test system was taken as the base case with the only change from [15] being the setting of all SGs' inertia constants to an equivalent 6.5 s.

Of interest in this work is the impact of CIG on the locational small-signal variability of voltage magnitude and frequency. As such, the SGs in area 2 are first replaced by GFLs and then by GFMs. Finally, the GFMs are instead placed in area 1 which results in a case which clarifies the capability of the method to focus on particular timescales of interest. The parameters associated with GFLs and GFMs are summarised in Table I. Note, per unit values are on the generator bases of 900 MVA and 20 kV, as is the case with the SGs.

TABLE I: Parameters for Converter-Interfaced Generation

CIG type	Parameter	Symbol	Value
Both	RLC resistance	R_f	0.03 pu
Both	RLC inductive reactance	$X_{l,f}$	0.08 pu
Both	RLC capacitive reactance	$X_{c,f}$	13.51 pu
Both	Power filter time constant	τ_p	0.0318 s
Both	Switching frequency	f_s	10 kHz
Both	ICC proportional gain, integral gain	K_P^{cc}, K_I^{cc}	$\{0.2122, 30\}$ V_{pu}/A_{pu}
GFL	APC proportional gain, integral gain	K_P^{apc}, K_I^{apc}	$\{0.02122, 3\}$ A_{pu}/MW_{pu}
GFL	RPC proportional gain, integral gain	K_P^{rpc}, K_I^{rpc}	$\{0.0118, 1.6667\}$ A_{pu}/MVA_{pu}
GFL	PLL proportional gain, integral gain	K_P^{pll}, K_I^{pll}	$\{20, 25\}$ rad/s/V_{pu}
GFM	APC virtual inertia, virtual damping	H, K_D	6.5 s, 10 pu
GFM	VMC reactive power droop	m_q	0.1%
GFM	Virtual resistance, virtual inductive reactance	$R_{vi}, X_{l,vi}$	0 pu, 0.2 pu

V. Results

The visualisation approach for the MAMC is a 3-dimensional bar graph. For these plots, the "disturbed bus"-axis displays the disturbance location, allowing visualisation of areas in which the the system is excited. The "observed bus"-axis refers to the location at which the variability is being "measured", or observed. That is, we can observe the buses which display the most variability after a disturbance at any given bus. The buses have been reordered on these axes to represent the layout of the system (Fig. 3).

The data generated by the case studies, from which the following analysis is performed, can be found in [26].

A. Validation of MAMC as a Variability Metric

1) Single-machine infinite bus (SMIB): By reducing the system to a SMIB with a single mode, we ensure that the output response is equal to the modal response. As such, the MAMC should be equal to the maximum deviation of the output following the specified disturbance. To test this, a SMIB system is considered with the synchronous generator classical model. The synchronous reactance of the machine was set to 0.3 pu and the inertia and damping constants were 3.5 s and 10 pu. The Thévenin equivalent reactance of the grid was set to 0.65 pu. The initial conditions included the 60 Hz grid frequency, the active and reactive power outputs of 0.9 pu and 0.3 pu, respectively, as well as the infinite bus and SG terminal voltages of 0.995 pu and $1\angle 36^\circ$ pu, respectively.

The responses to the SG rotor speed, ω_r, and the output electrical torque, T_e, were simulated using the MATLAB `impulse()` [22] function for a disturbance to both the infinite bus frequency, ω_{ib} (of 1 rad/s) and voltage magnitude $V_{m,ib}$ (of 1 pu). The corresponding values calculated for the MAMC are summarised in Table II alongside the maximum deviation values obtained from the time-domain response and the error between the two metrics. It can be seen that the MAMC matches exactly the maximum deviation value obtained from the time-domain impulse response up to at least 4 decimal places, confirming the theoretical derivation of (19). Note, the sizes of disturbances applied are not realistic and only used for proof of concept.

TABLE II: SMIB Validation Results

Input / Output	MAMC	Time-Domain Maximum (TDM)	Error
ω_{ib} / ω_r	5.5493 rad/s	5.5493 rad/s	0
ω_{ib} / T_e	292.3498 pu	292.3498 pu	0
$V_{m,ib}$ / ω_r	0.9044 rad/s	0.9044 rad/s	0
$V_{m,ib}$ / T_e	34.3085 pu	34.3085 pu	0

2) Two-area system validation of locational trends: For a system with multiple modes, e.g., the base SG-only two-area system, the MAMC is not expected to match exactly the maximum deviation of the output. This is due to the output being a superposition of modal responses and the MAMC being an approximation based only on the most contributing mode at any given disturbance and observation location. However, we are interested in the comparative relationships between the voltage magnitude and frequency, at different locations. Therefore, in this section we investigate the correlation between the MAMC and the corresponding maximum deviation in the time-domain response, across buses. That is, the locational distribution of the *variability*.

The 3D bar graphs displaying the MAMC and time-domain response maximum deviation (TDRMD) for the bus frequencies in response to an active power disturbance are displayed in Fig. 4a and Fig. 4b, respectively. Note, qualitative assessment of how the MAMC variability metric relates to the time-domain response is further explored in Subection V-F.

The similarities in trends are immediately obvious, although, the disturbance applied to area 1 and observed in area 2 is slightly raised compared to the rest of the locations in the TDRMD compared to the MAMC results. To

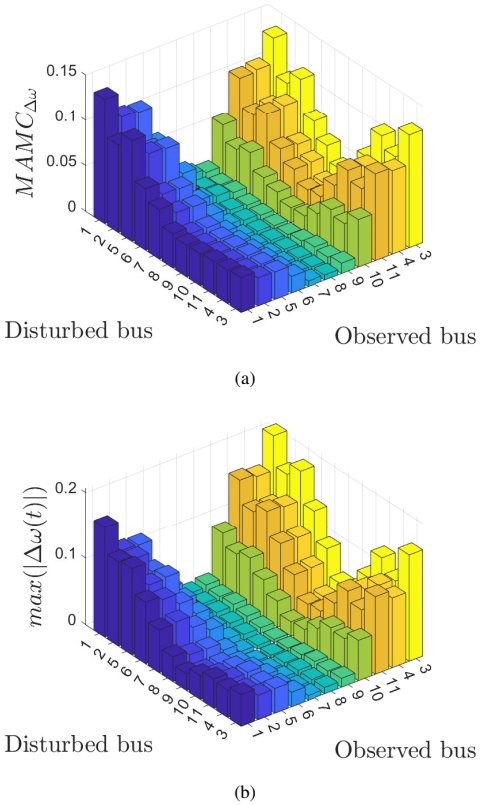

Fig. 4: (a) MAMC and (b) maximum deviation in time-domain of each bus frequency for an active power disturbance in the base SG-only system.

further highlight the matching in variability trends, the linear correlation coefficient (LCC) can be calculated between the arrays representing each disturbed bus. For example, there is an array for each disturbance location, whose elements are either the MAMC or TDRMD at each observed location. These arrays are referred to as the observational distributions. Note, that the opposite can also be done whereby there is an array for each observation bus location whose elements are the MAMC or TDRMD for each disturbance location. These arrays are referred to as the excitation distributions. The LCC was calculated using the MATLAB function `corr()` [22] which makes use of Pearson's metric. The LCC between the observational distributions of the MAMC and corresponding TDRMD for each disturbed bus is displayed in Fig. 5a. Similarly, the LCC between the excitation distributions follows in Fig. 5b. There is generally a good match with high LCC values observed. The result of the increase in variability for the TDRMD compared to the MAMC (visible in Fig. 4b), for a disturbance in area 1 observed in area 2, is that there is a dip in correlation for area 1 and area 2 in Fig. 5a and Fig. 5b, respectively.

By creating a single array which is the concatenation of all observational, or equivalently excitation, distribution arrays, we can determine the LCC between the two metrics for the variability trends as a whole. That is, comparing the full graphs in Fig. 4a and Fig. 4b. In this case, the resultant correlation coefficient is 0.9588. This will be termed the full LCC and is the accuracy measure used in the remainder of this work.

The same approach is applied when considering the voltage

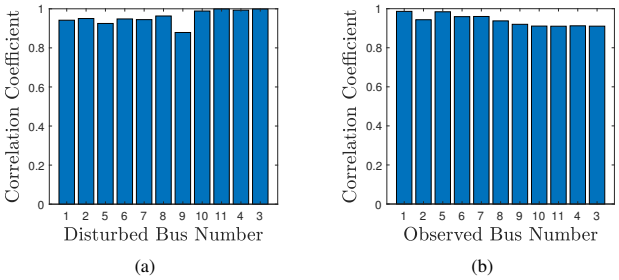

Fig. 5: Linear correlation coefficient between the MAMC and TDRMD of the (a) observational distributions and (b) excitation distributions for the frequency variability analysis in the base SG-only system.

magnitude at each bus as the output variable of interest. The resultant bar graphs for MAMC and TDRMD are shown in Fig. 6a and Fig. 6b, respectively.

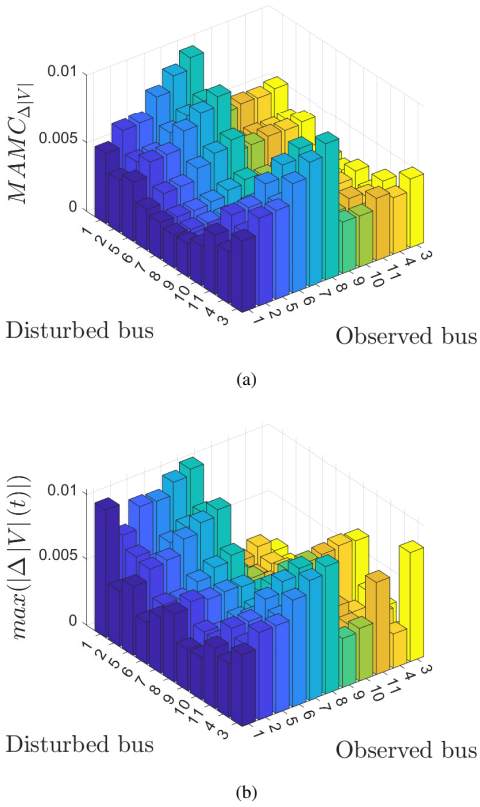

Fig. 6: (a) MAMC and (b) maximum deviation in time-domain of each bus voltage magnitude for an active power disturbance in the base SG-only system.

The errors in this case are more significant. In particular, there are peaks in the TDRMD that are not represented accurately by the MAMC which are observed in area 1 when area 1 is disturbed, and observed in area 2 when area 2 is disturbed (i.e., more local in nature). Similarly, there is slightly increased variability excited by a disturbance on bus 8 for all observed locations. Whereas the MAMC suggests there should be higher variability observed in area 2 when area 1 is disturbed. These deviations in the voltage results are reflected in the full LCC of 0.7644.

To observe the reasoning behind the lower performance in the case of voltages, the modal contributions (maximum

deviation of decoupled modal responses whose calculation is derived in Subsection II-C) in the areas with weakest matches can be investigated. When disturbing bus 1 and observing the same bus, several modes with similarly high values of contribution are identified. The main mode is oscillatory with a value of $-0.0703 \pm j3.2531$, which is in fact the expected interarea mode of the system [15], whose TDRMD occurs at approximately 0.51 s. However, there are also several non-oscillatory modes with sufficient contribution to influence the time-domain response, one in particular which has a value of $-30.4339 \pm j0$. On its own, this eigenvalue has just less modal contribution than the interarea mode but when combined with the other non-oscillatory modes, whose peaks all occur at the instance of the disturbance, the contribution becomes higher but is not accounted for in the MAMC (future work will look to improve the accuracy of the method through modal combination techniques, which may also be required for cases in which repeated eigenvalues occur [14]). This is illustrated in Fig. 7 whereby the voltage magnitude deviation is initially brought to -0.01 at the instance of the (active power impulse) disturbance due to the non-oscillatory modes which then damp out quickly leaving the interarea mode to dominate the response. However, noting the fast damping time constant of the non-oscillatory mode mentioned, it can be found that delaying the start of the measurement for TDRMD by 0.05 s gives a result which the MAMC matches much better with a full LCC of 0.9258. As such, the lack of modal combination approach means that some information is lost but the MAMC is still seen to identify some of the main underlying trends. More importantly, the method can be used to identify underlying reasons between the discrepancies and help in understanding their importance (or lack thereof).

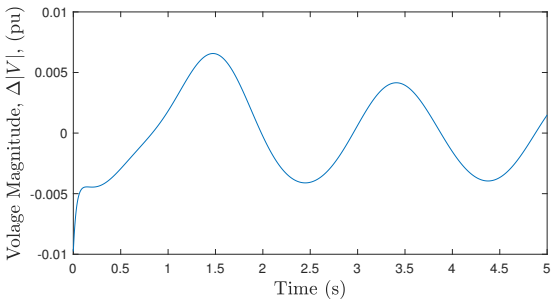

Fig. 7: Response of voltage magnitude at bus 1 to 0.1 pu active power disturbance at bus 1 in SG-only system.

Having highlighted the capability of the MAMC to reflect interesting variability trends, in addition to particular limitations, variability analysis is performed using the developed approach on the case studies from Section IV.

B. Variability Analysis of the Base Kundur Two Area System (SG-Only)

Fig. 4a reveals that for the base system, increased frequency variability is exhibited primarily when a disturbance is applied close to the SG locations (except for the observed variability in area 1 when area 2 is excited). When said disturbance occurs in area 1, the variability is observed mostly near the SGs in area 1 and in area 2; however, when the disturbance is applied in area 2, the variability is excited near the generators in area 2 but does not propagate to area 1. The highest contributing mode in the former case for both areas is a 0.145 Hz oscillation with the PFs revealing that it is related to the damper windings and rotor speed of the SG in area 1 and, to a lesser but still significant extent, area 2. An important note here is that this mode has a damping ratio of 0.86 and so would often be ignored in traditional small-signal analyses and stability metric-focused grid strength indicators such as the generalized short-circuit ratio [11]. Nevertheless, this is the mode that causes high amplitude deviations in the time domain responses of frequency throughout the system which can be revealed by observing the maximum deviations of the decoupled modal responses. For a disturbance in area 2, the variability observed in area 1 has most contribution from the 0.145 Hz oscillation but to a lesser extent than the disturbance in area 1. Also, the observed variability in area 2 is caused mostly by the system's interarea mode. Focusing on the mode shape of this interarea oscillation, its observability is focused on the rotor speed states of the SGs in area 2 with limited observability in area 1, hence the fact that the 0.145 Hz oscillation is the most impactful in this area.

This ability to highlight different modes contributing most to the observed variability in different locations for the same disturbances is one of the key benefits of the proposed method. i.e., the MAMC is a measure of locational variability that is not restricted to focusing on a single mode. Using a PF-based analysis approach such as in [14] is very useful for understanding the relationship between a single mode and the outputs of interest; however, it will not reveal the locational trends of output variability that is the interest of this work.

As discussed previously, the voltage variability excited and observed in area 1 of Fig. 6a is mostly caused by the interarea mode. It is also the same mode contributing most to the observed voltage variability in area 1 when a disturbance is applied in area 2. The observed variability in area 2 is found to be a result of the 0.145 Hz mode mentioned earlier for disturbances in area 1 and a non-oscillatory mode of value $-30.43 \pm j0$ for disturbances in area 2. For any given disturbance location, the interarea mode is observed most in area 1 and has less impact in area 2, contrary to what was seen for the frequency variability analysis. Since the mode will be excited the same amount for the same disturbance, the difference lies in the observability of the mode on the frequency vs. the voltage magnitude of each bus, highlighting the distinctive variability characteristics between them.

C. Variability Analysis After Replacing Synchronous Generators in Area 2 with Grid-Following Converters

For this case, the full LCC for the MAMC of frequency and voltage are 0.8745 and 0.8142, respectively, highlighting generally good match.

In Fig. 8a it can be seen that frequency variability is observed most in area 2, where the SGs have been replaced with GFL converters. It is also in this area where disturbances are seen to excite variability the most. The mode contributing

most to the variability in this region is non-oscillatory with value of $-18.33 \pm j0$ and PFs suggesting it is related mostly to the PLL angles of both GFLs and the outer active power controller of GFL3. For contrast, the mode contributing most to the variability for disturbances in area 1 with observation in area 1 (i.e., area with SGs) is also non-oscillatory with value of $-0.0042 \pm j0$ but is related to the rotor speed states of the SGs.

From Fig. 8b it is clear that the most significant voltage variability is observed in area 2 in response to disturbances in area 2 (i.e., where GFL converters are placed). The most contributing mode in this region is non-oscillatory with value $-7.77 \pm j0$ and the PFs reveal that it is an interaction mainly between the active power controllers of the two GFLs.

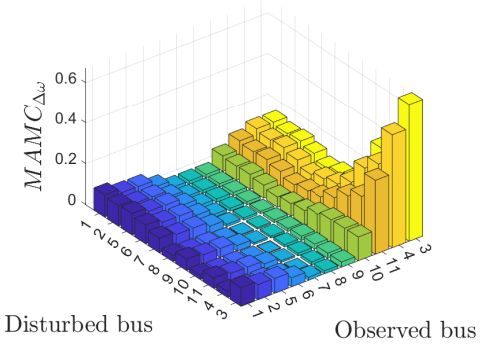

(a)

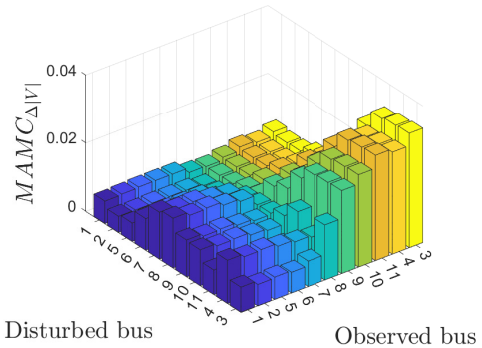

(b)

Fig. 8: MAMC for bus (a) frequencies and (b) voltage magnitude for an active power disturbance in the system with GFLs in area 2.

An important observation is that the most contributing modes for the majority (but not all) of disturbance and observational locations were non-oscillatory in this system. Therefore, care should be taken in systems with GFLs with respect to the potential for exacerbation of the MAMC limitations highlighted in Subsubsection V-A2. However, as mentioned previously, the full LCC highlighted the general validity of the MAMC in this specific scenario. It was also observed in [24] that non-oscillatory instability may become a more prevalent phenomenon in converter-dominated systems.

D. Variability Analysis After Replacing Synchronous Generators in Area 2 with Grid-Forming Converters

The full LCC for the MAMC of frequency and voltage for this case are 0.9010 and 0.8735, respectively, showing again a good match.

In Fig. 9a, the frequency variability trends are shown to be similar to the corresponding case of the SG-only system with the exception of less observed variability in area 2 in response to disturbances in area 2, where the GFMs have replaced the SGs. The cause of the variability for disturbances in area 1 and observation in area 1 is a non-oscillatory mode of $-0.86 \pm j0$ and is related primarily to the AVRs and damper windings of the SGs and small contribution from the virtual rotors of the GFMs. When observing area 2 after disturbances in area 1, it is primarily a mode of $-1.38 \pm j0.63$ which contributes most to the variability. The main PFs are of the damper windings and the AVRs of the SGs as well as the rotor speed of SG1 and small contributions from the virtual rotors of the GFMs. This mode also contributes heavily for disturbances in area 2. For such disturbances, when observing the variability in area 2, there is also a mode of $-0.38 \pm j3.04$ which contributes heavily, related to the GFMs' virtual rotors and, to a lesser extent, the SGs' rotors (i.e., the interarea mode). Although non-oscillatory modes do contribute to the variability in this case, the majority are oscillatory in nature, contrary to the case with the GFLs.

From Fig. 9b, a disturbance applied to area 1 is found to cause voltage variability much more in area 1 than in area 2. However, a disturbance in area 2 is seen to excite variability in both area 1 and area 2 and especially towards the centre of the system at bus 8. There is also seen to be significant values of MAMC observed in area 1 in response to a disturbance of the buses between the area 1 SG locations and the central bus 8. Analysis of the most contributing modes for disturbance to observation location, respectively, reveals that: area 1 to area 1 is caused mostly by the $-0.86 \pm j0$ mentioned previously; area 2 to area 2 is caused by an oscillatory mode with very fast damping and value of $140.25 \pm j0.60$, which is related to the ICCs of the GFMs; area 2 to area 1 is a result of the interarea mode ($-0.38 \pm j3.04$); and finally, the area 1 central region to area 1 more generally is caused by a non-oscillatory mode of value $-14.94 \pm j0$, related to the AVRs of the SGs.

E. Influence of Introducing GFLs and GFMs on the Base Case Modes That Contribute Most to Variability

As shown in Subsections V-C and V-D, the introduction of GFLs and GFMs can significantly affect the variability observed in the system in both frequency and voltage. In addition, the dynamic phenomena driving the observed variability can also be different, notably also affected significantly by non-oscillatory modes.

From the frequency variability analysis in Subsection V-B, two main modes which contributed strongly to variability were identified: the interarea mode (≈ 0.517 Hz) and the ≈ 0.145 Hz oscillation. Therefore, this subsection looks to establish how the introduction of GFLs and then GFMs to area 2 has impacted these modes. A summary is displayed in Table III. A key observation from this analysis is the potential for very different modal contributions, even when a mode has very similar eigenvalue characteristic (i.e., frequency and damping).

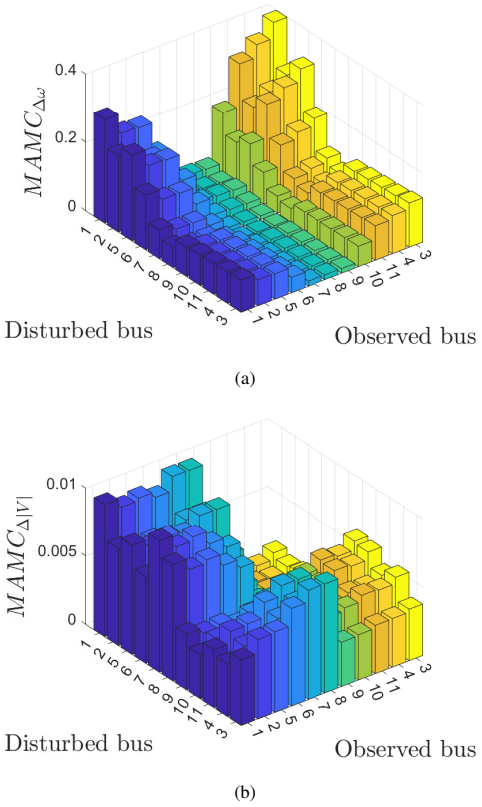

Fig. 9: MAMC for bus (a) frequencies and (b) voltage magnitude for an active power disturbance in the system with GFMs in area 2.

1) GFLs in area 2: The mode that has most similar characteristics to the ≈ 0.517 Hz mode in this case can be seen in Table III and has PFs showing an interaction between the SGs' rotors and the GFLs' PLLs, APCs, and RPCs. It is noted that this mode has slightly reduced frequency and much better stability margin (real part of mode). Additionally, the corresponding overall contribution, measured as an average of the absolute modal contribution (maximum deviation) across all disturbance and observational locations, is increased in this case compared to the base case (8.7 vs. 0.417). The fact that this mode was not highlighted in Subsection V-C highlights the extent to which the non-oscillatory modes were contributing. On the other hand, the ≈ 0.145 Hz mode is still present with PF-derived characteristics similar to those of the base case. However, this mode is found to have less average contribution across all disturbance and observational locations with 6.2 compared to its base case counterpart which has 12.6.

2) GFMs in area 2: In this case the interarea mode exists as an interaction between the GFMs' virtual rotors and, to a lesser extent, the SGs' rotors. It is found to have improved stability margin compared to the equivalent in the base case. This also has (slightly) increased average contribution, of 0.424. The mode most similar to the ≈ 0.145 Hz oscillation of the base case, in terms of value and dominant PFs, is the $-1.38 \pm j0.63$ mode mentioned previously. This in fact has increased average contribution as might be expected from its significant influence described in Subsection V-D.

TABLE III: INFLUENCE OF INTRODUCING GFLS AND GFMS ON THE KEY MODES OF THE BASE CASE

	Eigenvalue | Average $AMC_{\Delta\omega}$ $(\times 10^{-3})$*	
System	**$\approx$0.517 Hz mode**	**$\approx$0.145 Hz mode**
SGs-only	$-0.07 \pm j3.25$ | 0.417	$-1.52 \pm j0.91$ | 12.6
GFLs in area 2	$-1.56 \pm j2.83$ | 8.7	$-1.43 \pm j0.92$ | 6.2
GFMs in area 2	$-0.38 \pm j3.04$ | 0.424	$-1.38 \pm j0.63$ | 24.4

*$AMC_{\Delta\omega}$ = absolute modal contribution to frequency output. Average of which is across all disturbance and observational locations.

F. Variability Over Different Timescales

Swapping the GFMs to area 1 in addition to replacing the static reference calculation in Fig. 2 with an inner voltage controller (IVC)[1] revealed a scenario in which the variability across timescales can vary significantly and hence is useful for illustrative purposes. The response of the voltage magnitude at each bus in said system is displayed in Fig. 10 for a 0.1 pu active power disturbance at bus 1. For around the first second, the responses of the buses in area 1 are dominated by a relatively high frequency oscillation which subsequently damps out leaving a slower oscillation as the dominant mode, as the simulation continues. For the responses in area 2, the high frequency mode has less of an impact and it is the slower mode that dominates the responses.

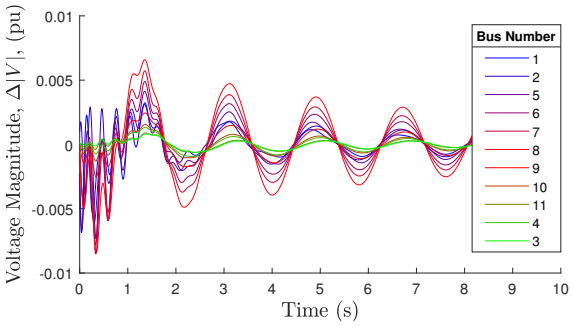

Fig. 10: Response of voltage magnitude to 0.1 pu active power disturbance at bus 1 in the system with GFMs in area 1.

To highlight the effect of these two distinct timescales, the MAMC is calculated twice: once considering only modes whose damping time constant was 1 s or less and again with consideration only of modes whose damping time constant was above 1 s, i.e., decoupling the fast and slow phenomena shown in Fig. 10. The resultant voltage magnitude MAMC for each observed bus is displayed in Fig. 11a and Fig. 11b for the two scenarios, respectively. For the former case, the variability is observed most in area 1 and the mode most contributing is a high frequency oscillation of value $-1.78 \pm j20.89$ with participation from the GFMs' ICCs and IVCs. The variability observed in area 2 is lesser with the most contributing mode this time found to be the slow interarea mode. This agrees with the qualitative analysis of the first second of the response in Fig. 10. When evaluating Fig. 11b it is seen that the maximum variability occurs at the central bus 8 with lesser variability occurring at the generator locations. The most contributing

[1]The proportional and integral gains of the IVC are tuned using the symmetrical optimum technique [23] and have values of 0.0813 pu and 13.9637 pu, respectively. The IVC also has decoupling and feed-forward terms (the latter of which is not present on the ICC in this case to enhance the stability of the system [27]).

mode for the observed variability for all buses except bus 3 and 4 have contribution most from the interarea mode. For bus 3 and bus 4 it is a very low frequency mode of value $-0.48 \pm j0.31$ that impacts the variability the most. Again, this agrees with the qualitative assessment of Fig. 10.

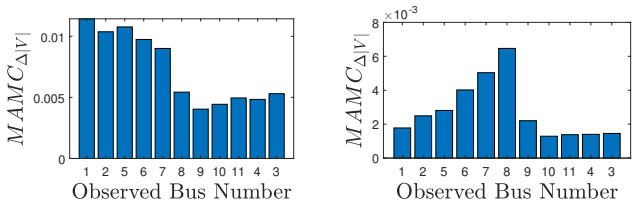

Fig. 11: MAMC for the voltage magnitude variability at each observed bus in response to a disturbance on bus 1–in the system with GFMs in area 1–for the timescale of (a) less than, and (b) more than 1 s.

Analysis of the MAMC for differing timescales is seen to reflect the changing nature of variability through time as well as allowing us to identify the specific modal interactions that are contributing to the variability at these different timescales. This can offer useful insights, especially for systems with high penetration of converters where higher frequency modes (in particular, sub-synchronous oscillations) can appear and become more prominent as seen in real world examples [28].

VI. Conclusions

This paper outlines an approach for studying small-signal variability of voltage magnitude or frequency at any given bus, for chosen disturbance locations. A metric is derived called the maximum absolute modal contribution (MAMC), which uses the analytical solution of the individual modal responses. This approach goes beyond typical system static strength metrics, capturing the effect on voltage and frequency variation of complex power system dynamics, in systems with high CIG penetration and different types of control (e.g., GFL and GFM). In particular, it was shown that the approach will capture, and hence highlight, dynamics which may be neglected using stability metrics such as the damping ratio which can have significant impact on the variability of the output. Additionally, the benefits of the proposed metric not focusing on a single mode are highlighted through the fact that a range of modes can contribute most to the variability at different disturbance and observation locations. The link between the MAMC and the mode contributing most to the variability was used throughout to gain an in-depth understanding of the causes of output variability. Furthermore, the need to investigate voltage magnitude and frequency variability separately, as the proposed method enables, is reinforced by showing distinct differences in frequency/voltage variability trends, driven by different phenomena.

The proposed method and metric is first validated on a simple single machine-infinite bus system and then applied to the Kundur two-area system. GFLs were then introduced and it was found that the modes contributing most to the variability of voltage magnitude and frequency were often non-oscillatory, strengthening the hypothesis seen in prior literature that these types of eigenvalues may become more influential in CIG-dominated systems. When GFMs were introduced, there was again increased contribution from non-oscillatory modes but to a lesser extent. An interesting finding was that the frequency variability as observed across observation and disturbance locations was similar for the SG-only case and the case when GFMs are introduced. However, when the GFLs are introduced, the frequency variability was much more concentrated for disturbances and observation in the area in which the GFLs were placed. For both scenarios the modes that contributed most to the variability of the output variables were discussed based on their PF characteristics. Further to this, it was shown how the introduction of GFLs or GFMs to the system can influence the contribution that certain modes provide to the output variability, without necessarily altering their frequency and damping characteristics.

Finally, the capability and importance of focusing on different timescales has been studied. Separating the modes included in the variability metric calculation and analysis by damping time constant reveals the different locational variability trends as time evolves. Also, it allows the most influential mode at different time periods to be identified.

VII. References

[1] O. Damanik, O. C. Sakinci, G. Grdenic, and J. Beerten, "Evaluation of the use of short-circuit ratio as a system strength indicator in converter-dominated power systems," in *2022 IEEE PES Innovative Smart Grid Technologies Conference Europe (ISGT-Europe)*, 2022.

[2] C. Henderson, A. Egea-Àlvarez, P. Papadopoulos, R. Li, L. Xu, R. D. Silva, A. Kinsella, I. Gutierrez, and R. Pabat-Stroe, "Exploring an impedance-based scr for accurate representation of grid-forming converters," in *IEEE Power & Energy Society General Meeting*, 2022.

[3] W. Dong, H. Xin, D. Wu, and L. Huang, "Small signal stability analysis of multi-infeed power electronic systems based on grid strength assessment," *IEEE Transactions on Power Systems*, vol. 34, pp. 1393–1403, 2019.

[4] Y. Gu and T. C. Green, "Power system stability with a high penetration of inverter-based resources," *Proceedings of the IEEE*, vol. 111, no. 7, pp. 832–853, 2023.

[5] M. Paolone, A. Monti, T. Gaunt, T. V. Cutsem, X. Guillaud, V. Vittal, M. Liserre, C. Vournas, and S. Meliopoulos, "Fundamentals of power systems modelling in the presence of converter-interfaced generation," *Electric Power Systems Research*, vol. 189, p. 106811, 2020.

[6] M. Cheah-Mane, A. Egea-Àlvarez, E. Prieto-Araujo, H. Mehrjerdi, O. Gomis-Bellmunt, and L. Xu, "Modeling and analysis approaches for small-signal stability assessment of power-electronic-dominated systems," *WIREs Energy and Environment*, p. e453, 2022.

[7] Y. Zhu, T. C. Green, X. Zhou, Y. Li, D. Kong, and Y. Gu, "Impedance margin ratio: a new metric for small-signal system strength," *TechRxiv*, 2023. [Online]. Available: https://doi.org/10.1109/TPWRS.2024.3371231

[8] U. Markovic, O. Stanojev, P. Aristidou, and G. Hug, "Partial grid forming concept for 100% inverter-based transmission systems," in *2018 IEEE Power & Energy Society General Meeting (PESGM)*. IEEE, 2018.

[9] E. Rokrok, T. Qoria, A. Bruyere, B. Francois, and X. Guillaud, "Classification and dynamic assessment of droop-based grid-forming control schemes : Application in hvdc systems," *Electric Power Systems Research*, vol. 189, p. 106765, 2020.

[10] F. Milano and Álvaro Ortega, "Frequency divider," *IEEE Transactions on Power Systems*, vol. 32, pp. 1493–1501, 2017.

[11] C. Liu, H. Xin, D. Wu, H. Gao, H. Yuan, and Y. Zhou, "Generalized operational short-circuit ratio for grid strength assessment in power systems with high renewable penetration," *IEEE Transactions on Power Systems*, pp. 1–15, 2023.

[12] C. Yang, L. Huang, H. Xin, and P. Ju, "Placing grid-forming converters to enhance small signal stability of PLL-integrated power systems," *IEEE Transactions on Power Systems*, vol. 36, pp. 3563–3573, 2021.

[13] D. Brahma and N. Senroy, "Sensitivity-based approach for assessment of dynamic locational grid flexibility," *IEEE Transactions on Power Systems*, vol. 35, pp. 3470–3480, 2020.

[14] G. Tzounas, I. Dassios, and F. Milano, "Modal participation factors of algebraic variables," *IEEE Transactions on Power Systems*, vol. 35, no. 1, pp. 742–750, 2020.

[15] P. S. Kundur, *Power System Stability and Control*, 3rd ed., N. J. E. L. Mark G. (EPRI) Balu, Ed. McGraw-Hill, 2017.

[16] K. Ogata, *Modern Control Engineering*, 5th ed. Upper Saddle River, New Jersey: Prentice Hall, 2010.

[17] C. Li, S. Wang, and J. Liang, "Tuning method of a grid-following converter for the extremely-weak-grid connection," *IEEE Transactions on Power Systems*, vol. 37, pp. 3169–3172, 2022.

[18] A. Egea-Àlvarez, S. Fekriasl, F. Hassan, and O. Gomis-Bellmunt, "Advanced vector control for voltage source converters connected to weak grids," *IEEE Transactions on Power Systems*, vol. 30, pp. 3072–3081, 2015.

[19] P. W. Pai and M. A. Sauer, *Power System Dynamics and Stability*. The University of Illinois, 1997. [Online]. Available: https://courses.engr.illinois.edu/ece576/sp2018/SauerandPaibook-Jan2007.pdf

[20] I. J. Perez-arriaga, G. C. Verghese, and F. C. Schweppe, "Selective modal analysis with applications to electric power systems, part i: Heuristic introduction," *IEEE Transactions on Power Apparatus and Systems*, vol. PAS-101, no. 9, pp. 3117–3125, 1982.

[21] A. K. Chopra, *Dynamics of Structures: Theory and Applications to Earthquake Engineering*, 4th ed. Upper Saddle River N.J: Prentice Hall, 2012.

[22] "Matlab version: 9.11 (r2021b)," Natick, Massachusetts, United States, 2021. [Online]. Available: https://www.mathworks.com

[23] C. Bajracharya, M. Molinas, J. A. Suul, and T. M. Undeland, "Understanding of tuning techniques of converter controllers for VSC-HVDC," in *Proceedings of the Nordic Workshop on Power and Industrial Electronics (NORPIE/2008)*, 2008.

[24] U. Markovic, O. Stanojev, P. Aristidou, E. Vrettos, D. Callaway, and G. Hug, "Understanding small-signal stability of low-inertia systems," *IEEE Transactions on Power System*, vol. 36, pp. 3997–4017, 2021.

[25] M. Beza and M. Bongiorno, "Impact of converter control strategy on low- and high-frequency resonance interactions in power-electronic dominated systems," *International Journal of Electrical Power & Energy Systems*, vol. 120, p. 105978, 2020.

[26] L. Benedetti, A. Egea-Àlvarez, and P. Papadopoulos, "Results data: A modal contribution metric for quantifying small-signal variability in power systems with converter-interfaced generation," figshare, Jul 2024, doi:10.48420/26412331. [Online]. Available: https://figshare.manchester.ac.uk/articles/dataset/_/26412331/0

[27] T. Qoria, F. Gruson, F. Colas, X. Guillaud, M.-S. Debry, and T. Prevost, "Tuning of cascaded controllers for robust grid-forming voltage source converter," in *2018 Power Systems Computation Conference (PSCC)*, 2018, pp. 1–7.

[28] Y. Cheng, L. Fan, J. Rose, S.-H. Huang, J. Schmall, X. Wang, X. Xie, J. Shair, J. R. Ramamurthy, N. Modi, C. Li, C. Wang, S. Shah, B. Pal, Z. Miao, A. Isaacs, J. Mahseredjian, and J. Zhou, "Real-world subsynchronous oscillation events in power grids with high penetrations of inverter-based resources," *IEEE Transactions on Power Systems*, vol. 38, no. 1, pp. 316–330, 2023.

Luke Benedetti (Member, IEEE) received the B.Eng. degree from the Department of Electronic and Electrical Engineering, University of Strathclyde, Glasgow, Scotland, in 2020. He is currently working towards the Ph.D. degree at the same institution. He is also currently a Research Associate with the Department of Electrical and Electronic Engineering, University of Manchester, Manchester, U.K. His research interests include the dynamics, stability, and control of power systems permeated with power electronic-interfaced devices.

Panagiotis N. Papadopoulos (S'05-M'14) is a Reader (Associate Prof.) in the Department of Electrical and Electronic Engineering at the University of Manchester and a UK Research and Innovation Future Leaders Fellow. He received the Dipl. Eng. and Ph.D. degrees from the Department of Electrical and Computer Engineering at Aristotle University of Thessaloniki, in 2007 and 2014, respectively. From 2014-2017, he was a post-doctoral Research Associate at the University of Manchester and in 2017, he joined the University of Strathclyde as a Lecturer. His research interests are in the area of power system stability and dynamics under increased uncertainty, introduced due to the integration of new technologies. He is also interested in power system applications of machine learning to tackle complex problems related to power system stability.

Agustí Egea-Àlvarez is a Professor at the electronic & electrical engineering department and, a member of the PEDEC (Power Electronics, Drives and Energy Conversion) group at the University of Strathclyde, Glasgow, U.K. He is also Network Operational Performance Manager at ScottishPower Energy Networks. Also, he was a holder of a Royal Academy of Engineering Industrial Fellowship between 2022 and 2024. He obtained his BSc, MSc and PhD from the Technical University of Catalonia in Barcelona in 2008, 2010 and 2014 respectively. In 2015, he was a Marie Curie fellow at the China Electric Power Research Institute (CEPRI). In 2016, he joined Siemens Gamesa as a converter control engineer working on grid-forming controllers and alternative HVDC schemes for offshore wind farms. He is a member of IEEE and IET and has been involved in several CIGRE working groups.